Journal of Mathematical Biology (2020) 80:1389–1411
https://doi.org/10.1007/s00285-020-01466-1

Mathematical Biology

Localized outbreaks in an S-I-R model with diffusion

Chunyi Gai[1] · David Iron[1] · Theodore Kolokolnikov[1]

Received: 15 April 2019 / Revised: 31 December 2019 / Published online: 16 January 2020

Abstract
We investigate an SIRS epidemic model with spatial diffusion and nonlinear incidence rates. We show that for small diffusion rate of the infected class D_I, the infected population tends to be highly localized at certain points inside the domain, forming K spikes. We then study three distinct destabilization mechanisms, as well as a transition from localized spikes to plateau solutions. Two of the instabilities are due to coarsening (spike death) and self-replication (spike birth), and have well-known analogues in other reaction–diffusion systems such as the Schnakenberg model. The third transition is when a single spike becomes unstable and moves to the boundary. This happens when the diffusion of the recovered class, D_R becomes sufficiently small. In all cases, the stability thresholds are computed asymptotically and are verified by numerical experiments. We also show that the spike solution can transit into an plateau-type solution when the diffusion rates of recovered and susceptible class are sufficiently small. Implications for disease spread and control through quarantine are discussed.

Mathematics Subject Classification 35B36 · 35Q92 · 92D25

1 Introduction

The SIRS epidemic model introduced by Kermack and McKendrick in 1927 Kermack and McKendrick (1927) is widely used to model the spread of infectious diseases. The population is divided into three disjoint classes: susceptible (S), infected (I), and recovered (R), where susceptibles can be infected by those already infected and subsequently recover, and recovered class are immune to the disease but lose immunity

✉ Theodore Kolokolnikov
tkolokol@gmail.com

[1] Department of Mathematics and Statistics, Dalhousie University, Halifax, Canada

over time. These assumptions are modelled using the following system of ODEs:

$$\begin{cases} S_t = -\beta SI + \gamma R, \\ I_t = \beta SI - \nu I, \\ R_t = \nu I - \gamma R, \end{cases} \tag{1}$$

where β is the infection rate, ν is the recovery rate, and γ is the rate of immunity loss. Kermack and McKendrick's work has motivated the use of mathematics in the study of epidemiology (Feng and Velasco-Hernández 1997; Hethcote 2000; van den Driessche and Watmough 2000).

While spatially-homogeneous dynamics are by now well studied, modelling spatial interactions is still an active area of research. Most disease outbreaks have a strong spatial characteristic, and many studies emphasize the importance of the spatial dimension for modelling these outbreaks. For example, Zulu et al. (2014) looked at spatio-temporal patterns in HIV outbreaks in Malawi over two decades (1994–2010). The authors found that the disease initially spread in several localized hot-spots and they identified several geographically differentiated HIV/AIDS epidemics rather than a single one. These initial outbreaks were followed by a complex spatio-temporal dynamics. Similar spatial clusters of HIV outbreaks were found in a recent study (Jeefoo 2012) in Phayao Province, Thailand, and in South Africa (Tanser et al. 2009).

In recent decades, numerous methodologies have been used to describe spatial distribution of disease. This include the use of cellular automata (Doran and Laffan 2005; Fuks and Lawniczak 2001), metapopulations (Arino and Van den Driessche 2003; Arino et al. 2007; Lloyd and Jansen 2004), networks (Kuperman and Abramson 2001; Yuan and Chen 2008) and partial differential equations (Murray 2001; Sun 2012). Generally speaking, incorporating spatial structure leads to very rich dynamics in epidemic models, such as formation of disease hot-spots.

In this paper we study spatially-localized outbreaks for the SIRS model with spatial dispersion. As will be shown below, such outbreaks can occur when the infection rate β is nonlinear. For simplicity, we will assume that β is proportional to I, although other types of nonlinearity, such as Holling functional response also lead to hot-spot formation. We model spatial dispersion using diffusion. This results in the following system,

$$\begin{cases} S_t = D_S S_{xx} - \chi SI^2 + \gamma R, \\ I_t = D_I I_{xx} + \chi SI^2 - \nu I, \\ R_t = D_R R_{xx} + \nu I - \gamma R. \end{cases} \tag{2}$$

Here D_S, D_I, D_R are diffusion coefficients of each class of population, χI is the rate of infection. We study the epidemic system on 1-D interval $[-L, L]$ with Neumann boundary conditions, so that $S_x = I_x = R_x = 0$ at $x = \pm L$. For simplicity, we also assume the timescale of infection and recovery is much shorter than the average life span, so birth and death rates for each class are neglected.

The second key assumption we make is that the infected class I diffuses more slowly than others. There are two scenarios where this is biologically plausible. The first scenario, common in many species is that the disease itself reduces the species mobility. A second scenario, applicable to humans, is an intentional quarantine policy to limit the

spread of infection. Such a policy is well known to be effective in controlling disease outbreaks and is often used a first-line defense against quickly-spreading infections.

We therefore write $D_I = \varepsilon^2$ where ε is small. By further rescaling,[1] we may set $\chi = 1, \nu = 1$. This leads to the following singularly perturbed reaction diffusion system:

$$\begin{cases} S_t = D_S S_{xx} - SI^2 + \gamma R, \\ I_t = \varepsilon^2 I_{xx} + SI^2 - I, \\ R_t = D_R R_{xx} + I - \gamma R. \end{cases} \tag{3}$$

Under these assumptions, this system has localized disease concentrations corresponding to spike-type solutions. Such spike patterns have been studied in great detail since 1990's in simpler reaction–diffusion systems consisting of two components, such as Gierer–Meinhardt system, Gray–Scott model, Schnakenberg model and Keller–Segel model and its variants. We refer reader to Doelman et al. (2001), Kang et al. (2007), Kolokolnikov et al. (2005a), Kolokolnikov and Wei (2018), Iron et al. (2001), Iron and Ward (2002), Maini et al. (2012), Muratov and Osipov (2000, 2002), Painter and Hillen (2011), Sherratt and Lord (2007), Wei (1999) and Wei and Winter (2013) and references therein. The introduction of a third component leads to interesting new phenomena not present in two-component reaction–diffusion systems (Buttenschoen et al. 2019).

Let us summarize the main results in this paper. Simulations and analysis show that the behavior of the system is highly dependent on diffusion rate D_R, relative to the diffusion rate of infected class, ε^2. We isolate two distinct regimes: either $D_R \gg O(\varepsilon^2)$ or $D_R \leq O(\varepsilon^2)$.

The regime $D_R \gg O(\varepsilon^2)$ is studied in Sects. 2, 3 and 5. In this regime, the steady-state population consists of K hot-spots of disease, uniformly distributed inside the interval $[-L, L]$. Depending on system parameters, the K-spike steady state can undergo two types of instabilities. The first type, analyzed in Sect. 5.1 is referred to as *spike competition instability*. As a result of such an instability, some of the hot-spots are "absorbed" by others, resulting in fewer hot-spots. The second type of instability, studied in Sect. 5.2 is referred to as *self-replication instability*, whereby a spike splits into two, resulting in more spikes. These instabilities are illustrated in Fig. 1. Figure 1a shows 8 spikes that gradually coarsen into 2 as D_S is gradually increased. On the other hand, with one-spike equilibrium as initial condition, replication occurs and more spikes appear as we gradually decrease D_S. This is shown in Fig. 1b. We derive explicit thresholds for D_S such that the spike competition occurs when $D_S > D_{SK}^{com}$, $K \geq 2$; and self-replication instability occurs when $D_S < D_{SK}^{rep}$, $K \geq 1$. Formulas for D_{SK}^{com} and D_{SK}^{rep} are given in Sect. 5.

The second regime we study is when D_R is small: $D_R \leq O(\varepsilon^2)$. In this case, a single spike can become unstable, and depending on other parameters, two phenomena can occur. If D_R is sufficiently small, a single spike moves to the boundary (depending on how big D_S is), as illustrated in Fig. 2. This phenomenon is studied in Sect. 4. On the other hand, when both D_R and D_S are small, the spike "fattens up" and

[1] Let $t = \frac{\hat{t}}{\nu}$, $S = \sqrt{\frac{\nu}{\chi}}\hat{S}$, $I = \sqrt{\frac{\nu}{\chi}}\hat{I}$, $R = \sqrt{\frac{\nu}{\chi}}\hat{R}$ and define new parameters by $\gamma = \nu\hat{\gamma}$, $D_S = \nu\hat{D_S}$, $D_I = \nu\varepsilon^2$, $D_R = \nu\hat{D_R}$. Upon dropping the hats, this yields (3).

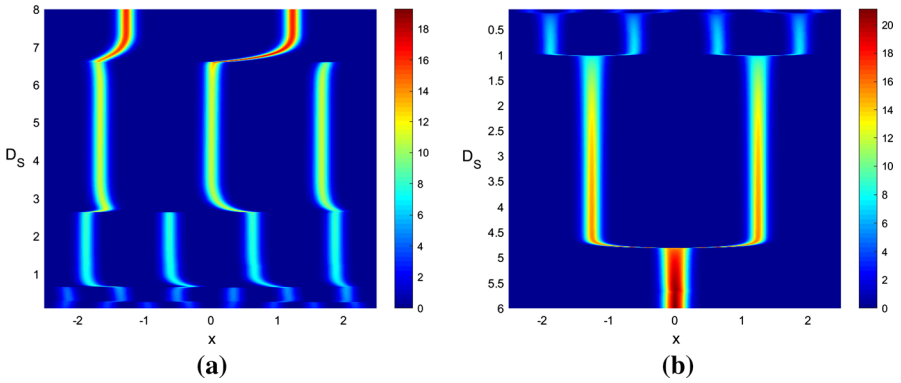

Fig. 1 Instabilities of steady state spike solutions induced by slowly increasing D_S or decreasing D_S. Here $D_R = 1, L = 2.5, \varepsilon = 0.05, N = 15$ and $\gamma = 1$. Left: coarsening (competition) instability when D_S is increased ($D_S = 1 + 10^{-5}t$). Colour plot of I is shown. Right: self-replication instability when D_S is slowly decreased ($D_S = 6 - 10^{-5}t$)

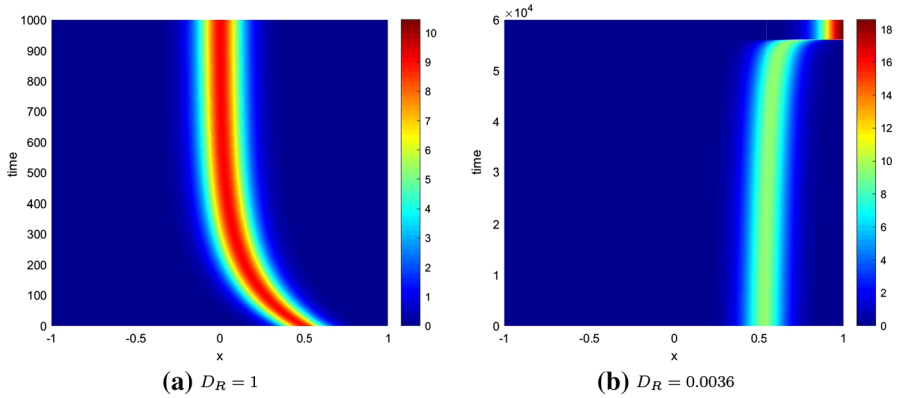

Fig. 2 Stable and unstable motion of a single spike. Here, D_R is as indicated while other parameters are fixed at $D_S = 5, L = 1, \varepsilon = 0.06, N = 5$ and $\gamma = 1$. In (**a**), one-spike equilibrium moves to the center, which shows that the center spike is stable. In (**b**) the spike moves to boundary instead of moving to center, so that a single spike is unstable

becomes a mesa-type pattern, i.e. a contiguous region of high concentration of disease connected via a sharp interface to a region of low concentration. Numerically we observe two types of inhomogeneous equilibrium depending on the value of D_S and an example of such a steady state pattern is shown in Fig. 3. Spike-type solution exists for sufficiently large D_S, but transition to interface-type patterns for small D_S. This process is illustrated in Fig. 3 (left). Interface patterns are studied in Sect. 6.

2 Single-spike solution

We start by constructing a single interior spike solution to (3). Such a solution corresponds to a localized concentration of the infected population I at some point x_0

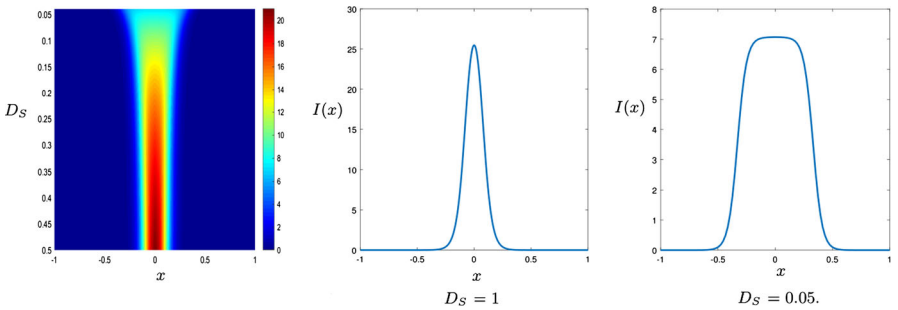

Fig. 3 Transition from spike to mesa when $D_R = 0, \varepsilon = 0.04, N = 10, L = 1, \gamma = 1$ with D_S as a control parameter. Left: D_S is gradually decreased from 0.5 to 0.05. Middle, Right: Profile of $I(x)$ for D_S as indicated

in the interior of the domain, $x_0 \in (-L, L)$. The extent of the spike is of $O(\varepsilon)$. We therefore introduce the inner variable

$$y = \frac{x - x_0}{\varepsilon}. \tag{4}$$

In the inner region, equilibrium solution of (3) then satisfies the system

$$\begin{cases} S_{yy} - \frac{\varepsilon^2}{D_S} S I^2 + \frac{\varepsilon^2}{D_S} \gamma R = 0, \\ I_{yy} + S I^2 - I = 0, \\ R_{yy} + \frac{\varepsilon^2}{D_R} I - \frac{\varepsilon^2}{D_R} \gamma R = 0. \end{cases} \tag{5}$$

We then expand S, I, R in ε as follows:

$$\begin{aligned} S &= S_0 + \varepsilon S_1 + O(\varepsilon^2), \\ I &= I_0 + \varepsilon I_1 + O(\varepsilon^2), \\ R &= R_0 + \varepsilon R_1 + O(\varepsilon^2). \end{aligned} \tag{6}$$

Upon substituting (6) into (5) and collecting higher-order terms in ε, we obtain, to leading order,

$$\begin{cases} S_{0yy} = 0, \\ I_{0yy} + S_0 I_0^2 - I_0 = 0, \\ R_{0yy} = 0. \end{cases} \tag{7}$$

This shows that S_0 and R_0 are constants to be determined. We then rescale

$$I_0 = \frac{1}{S_0} w(y), \tag{8}$$

where so that w satisfies the well-known ground-state

$$w'' - w + w^2 = 0, \; w \to 0 \text{ as } y \to \pm\infty$$

whose explicit solution is given by

$$w(y) = \frac{3}{2}\text{sech}^2\left(\frac{y}{2}\right).$$

To determine R_0 and S_0, we must match the inner and the outer region. In the outer region we approximate $I \sim \left(\int_{-L}^{L} I dx\right)\delta(x - x_0)$ and $SI^2 \sim \left(\int_{-L}^{L} SI^2 dx\right)\delta(x - x_0)$. We further estimate $\left(\int_{-L}^{L} I dx\right) \sim \frac{1}{S_0}\varepsilon\int_{-\infty}^{\infty} w dy \sim 6\varepsilon/S_0$ and similarly, $\int_{-L}^{L} SI^2 dx \sim 6\varepsilon/S_0$, so that

$$\begin{aligned} 0 &= D_S S_{xx} + \gamma R - 6\varepsilon/S_0\delta(x - x_0), \\ 0 &= D_R R_{xx} - \gamma R + 6\varepsilon/S_0\delta(x - x_0). \end{aligned} \tag{9}$$

To solve (9), we introduce the Green's function $G(x; x_0)$, which satisfies

$$G_{xx} - \mu^2 G = -\delta(x; x_0), \quad G_x(\pm L) = 0, \text{ where } \mu = \sqrt{\frac{\gamma}{D_R}}. \tag{10}$$

A simple calculation gives

$$G(x; x_0) = \frac{1}{\mu \sinh(2\mu L)} \begin{cases} \cosh(\mu(x + L))\cosh(\mu(x_0 - L)), & -L < x < x_0 \\ \cosh(\mu(x_0 + L))\cosh(\mu(x - L)), & x_0 < x < L. \end{cases} \tag{11}$$

The solution to (9) is then given by

$$R(x) = \frac{6\varepsilon}{S_0 D_R} G(x; x_0) \tag{12}$$

and

$$S(x) = \frac{D_R}{D_S}(R_0 - R(x)) + S_0, \tag{13}$$

where $R(x) = \frac{6\varepsilon}{S_0 D_R} G(x; x_0)$, $R_0 = R(0)$ and S_0 is to be determined.

To find S_0, we use the conservation of mass. Let N be the total population, so that

$$N \equiv \int_{-L}^{L} S + I + R dx. \tag{14}$$

Note that by adding three equations in (3) and integrating over the domain, N is independent of time. We will also take

$$N = 2N_0 L, \tag{15}$$

where N_0 is an arbitrary constant depending on initial conditions, so that N scales with domain size; N_0 can be thought of an average density.

We now substitute (8), (12) and (13) into the mass conservation condition (14, 15) to obtain that

$$S_0^2 - N_0 S_0 + E = 0, \tag{16}$$

where

$$E = \frac{3\varepsilon}{L}\left(1 + \frac{1}{\gamma} - \frac{D_R}{\gamma D_S} + 2\sqrt{\frac{D_R}{\gamma}}\frac{L}{D_S}\frac{\cosh\left(\sqrt{\frac{\gamma}{D_R}}(x_0+L)\right)\cosh\left(\sqrt{\frac{\gamma}{D_R}}(x_0-L)\right)}{\sinh\left(2\sqrt{\frac{\gamma}{D_R}}L\right)}\right). \tag{17a}$$

Solving (16) we get two roots when $N_0^2 - 4E > 0$; the system has no solution when $N_0^2 - 4E < 0$. Asymptotically in ε, they are

$$S_{0-} \sim \frac{E}{N_0}, \tag{17b}$$

which is of $O(\varepsilon)$ and

$$S_{0+} \sim N_0, \tag{17c}$$

which is of $O(1)$. Plots of these two roots are shown in Fig. 4. The two roots connect at a fold point corresponding to a double root of (16).

We now summarize our first result:

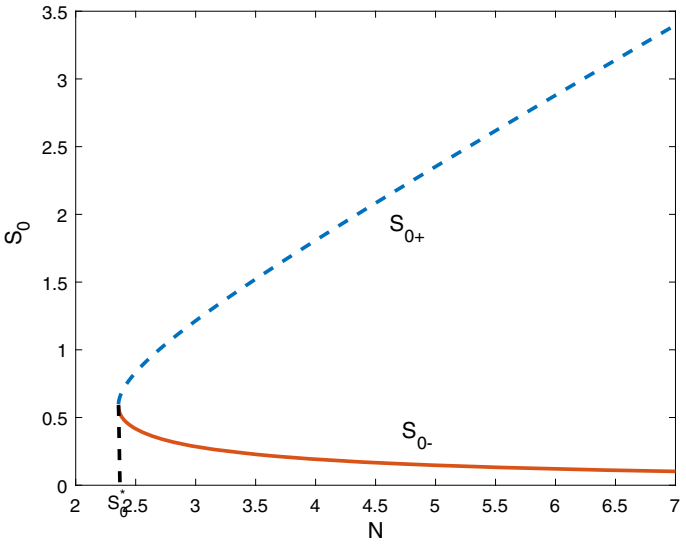

Fig. 4 Plot of two roots to (16) versus total population N. Here $\varepsilon = 0.05$, $L = 1$, $D_R = 1$, $D_S = 1$ and $\gamma = 1$. The dashed curve denotes S_{0+} and the solid curve denotes S_{0-}. S_0^* is the fold point where (16) has double root

Result 2.1 *In the limit $\varepsilon \to 0$, with D_R and D_S independent of ε, the SIRS system (3) has the following single-spike steady state:*

$$\begin{aligned} S(x) &\sim -\frac{6\varepsilon}{S_0 D_S} G(x; x_0) + \frac{6\varepsilon}{S_0 D_S} G(x_0; x_0) + S_0, \\ I(x) &\sim \frac{1}{S_0} w\left(\frac{x - x_0}{\varepsilon}\right), \\ R(x) &\sim \frac{6\varepsilon}{S_0 D_R} G(x; x_0), \end{aligned} \tag{18}$$

where $G(x; x_0)$ is given by (11), $w(y) = \frac{3}{2}\operatorname{sech}^2(\frac{y}{2})$ and S_0 is a constant determined by the total population mass as given in (17), assuming that the solution of (16) exists.

3 Nonlocal eigenvalue problem

We now study the stability of one-spike solution. We first linearize around the steady state by taking

$$\begin{aligned} S(x,t) &= S(x) + e^{\lambda t}\varphi(x), \\ I(x,t) &= I(x) + e^{\lambda t}\psi(x), \\ R(x,t) &= R(x) + e^{\lambda t}\xi(x). \end{aligned}$$

Assuming $|\varphi|, |\psi|, |\xi| \ll O(1)$ we obtain the linearized problem

$$\begin{cases} \lambda\varphi = D_S\varphi_{xx} - I_0^2\varphi - 2S_0 I_0\psi + \gamma\xi, \\ \lambda\psi = \varepsilon^2\psi_{xx} + I_0^2\varphi + (2S_0 I_0 - 1)\,\psi, \\ \lambda\xi = D_R\xi_{xx} + \psi - \gamma\xi. \end{cases} \tag{19}$$

with Neumann boundary conditions at $x = \pm L$.

In the inner region, we let $y = \frac{x - x_0}{\varepsilon}$ where x_0 is the spike position. To leading order, we then obtain $\varphi_{yy} \sim 0$ so that $\varphi(y) \sim \varphi_0$ is constant to be determined. The equation for ψ is

$$\lambda\psi = \psi_{yy} - \psi + 2w(y)\psi + I_0^2\varphi_0. \tag{20}$$

In the outer region, we approximate

$$\begin{cases} D_S\varphi_{xx} - \lambda\varphi + \gamma\xi = c_1\delta(x; x_0) \\ D_R\xi_{xx} - (\gamma + \lambda)\xi = c_2\delta(x; x_0) \end{cases} \tag{21}$$

where

$$c_1 = \varphi_0 \int I_0^2 dx + 2S_0 \int I_0\psi\, dx, \qquad c_2 = -\int \psi\, dx. \tag{22}$$

We write

$$\xi(x; x_0) = -\frac{c_2}{D_R} G\,(x; x_0)\,, \tag{23}$$

where $G(x; x_0, \mu)$ is the Green's function that satisfies (10), but with $\mu = \sqrt{\frac{\gamma+\lambda}{D_R}}$. To solve for φ, we make a change of variables. Let

$$\varphi = \frac{D_R \gamma}{\lambda(D_R - D_S) - \gamma D_S} \xi + \varphi_h. \tag{24}$$

Then φ_h satisfies:

$$D_S \varphi_{hxx} - \lambda \varphi_h = \left(c_1 - \frac{\gamma c_2}{\lambda(D_R - D_S) - \gamma D_S} \right) \delta(x; x_0)$$

so that

$$\varphi_h = -\frac{1}{D_S} \left(c_1 - \frac{\gamma c_2}{\lambda(D_R - D_S) - \gamma D_S} \right) G(x; x_0).$$

Therefore we estimate

$$\varphi_0 = \varphi(x_0) \sim -c_2 \frac{\gamma}{\lambda(D_R - D_S) - \gamma D_S} G\left(x_0; x_0, \sqrt{\frac{\gamma+\lambda}{D_R}} \right) - \frac{1}{D_S} \left(c_1 - \frac{\gamma c_2}{\lambda(D_R - D_S) - \gamma D_S} \right) G(x_0; x_0)$$

and

$$c_1 = \varepsilon \left(\frac{\varphi_0}{S_0^2} \int w^2 dy + 2 \int w \psi dy \right); \quad c_2 = -\varepsilon \int \psi dy. \tag{25}$$

After some algebra, this leads to the following non-local eigenvalue problem (NLEP),

$$(L_0 - \lambda)\psi = w^2 \frac{2}{\int_{-\infty}^{\infty} w^2 dy - (\lambda + 1)\frac{S_0^2}{\varepsilon P}} \int_{-\infty}^{\infty} w \psi dy, \tag{26}$$

$$\text{where } L_0 \psi = \psi_{yy} - \psi + 2w\psi \tag{27}$$

and where

$$P = \frac{\gamma \sqrt{\frac{D_R}{\lambda+\gamma}}}{\lambda(D_R - D_S) - \gamma D_S} \frac{\cosh\left(\sqrt{\frac{\lambda+\gamma}{D_R}} (x_0 + L) \right) \cosh\left(\sqrt{\frac{\lambda+\gamma}{D_R}} (x_0 - L) \right)}{\sinh\left(2\sqrt{\frac{\lambda+\gamma}{D_R}} L \right)} - \frac{\lambda + 1 + \frac{D_S \gamma}{\lambda(D_R - D_S) - \gamma D_S}}{\sqrt{\lambda D_S}} \frac{\cosh\left(\sqrt{\frac{\gamma}{D_S}} (x_0 + L) \right) \cosh\left(\sqrt{\frac{\gamma}{D_S}} (x_0 - L) \right)}{\sinh\left(2\sqrt{\frac{\gamma}{D_S}} L \right)}. \tag{28}$$

For the special case when $x_0 = 0$, this expression simplifies to

$$P(\lambda) = \frac{\gamma\sqrt{\frac{D_R}{\lambda+\gamma}}}{\lambda(D_R - D_S) - \gamma D_S} \frac{\coth\left(\sqrt{\frac{\lambda+\gamma}{D_R}}L\right)}{2} - \frac{\lambda + 1 + \frac{D_S\gamma}{\lambda(D_R-D_S)-\gamma D_S}}{\sqrt{\lambda D_S}} \frac{\coth\left(\sqrt{\frac{\gamma}{D_S}}L\right)}{2}. \tag{29}$$

In general, the NLEP problem (26) is difficult to tackle since P has such a complicated dependence on λ. However there are two cases for which stability of (26) is well established: namely, large or small $\frac{S_0^2}{\varepsilon}$. Note that S_0 is given by (17) and has two branches, S_{0+} and S_{0-}, refer to Fig. 4. Consider the case of large N. Then $\frac{S_{0+}^2}{\varepsilon} \gg 1$ whereas $\frac{S_{0-}^2}{\varepsilon} \ll 1$. In the former case, (26) reduces to a *local* eigenvalue problem $(L_0 - \lambda)\psi \sim 0$. This problem is well known to admit a positive eigenvalue $\lambda = 5/4$ corresponding to $\psi = \sqrt{w}$ (Lamb Jr 1980) so that this branch is unstable. For the latter case ($S_0 = S_{0-}$), the problem (26) reduces to the following well-known NLEP problem:

$$\lambda\psi = L_0\psi - 2w^2\frac{\int_{-\infty}^{\infty} w\psi dy}{\int_{-\infty}^{\infty} w^2 dy}, \quad S_0 \sim O(\varepsilon). \tag{30}$$

This is well-known to be *stable* as was first proven in Wei (1999).

Finally, a lengthy but a straightforward algebraic computation shows that at the fold point where $S_{0+} = S_{0-}$, there is a zero eigenvalue whose corresponding eigenfunction is given by $\psi = w$. This suggests that the entire branch S_{0+} is unstable whereas the entire branch S_{0-} is stable, although the proof of this fact is not in the cards due to the complex structure of $P(\lambda)$. This structure is analogous to the well-known properties of the Grey–Scott model in the low-feed regime (Kolokolnikov et al. 2005b).

4 Spike motion

We now study the motion of the interior spike, which is determined by small eigenvalues. We rewrite the system as following:

$$\begin{cases} S_t = D_S S_{xx} - SI^2 + \gamma R, \\ I_t = \varepsilon^2 I_{xx} + SI^2 - I, \\ R_t = D_R R_{xx} + I - \gamma R \end{cases} \tag{31}$$

with Neumann boundary conditions and $D_S, D_R \gg O(\varepsilon^2)$. To study the motion of the spike, we expand around the center x_0 by writing $x = x_0 + \varepsilon y$, and let $x_0 = x_0(\varepsilon^2 t)$, $S(y,t) = S\left(\frac{x-x_0(\varepsilon^2 t)}{\varepsilon}\right)$, $I(y,t) = I\left(\frac{x-x_0(\varepsilon^2 t)}{\varepsilon}\right)$, and $R(y,t) = R\left(\frac{x-x_0(\varepsilon^2 t)}{\varepsilon}\right)$. Then system (31) becomes

$$\begin{cases} -\varepsilon^3 x_0' S_y = D_S S_{yy} - \varepsilon^2 S I^2 + \varepsilon^2 \gamma R, \\ -\varepsilon x_0' I_y = I_{yy} + S I^2 - I, \\ -\varepsilon^3 x_0' R_y = D_R R_{yy} + \varepsilon^2 I - \varepsilon^2 \gamma R. \end{cases} \tag{32}$$

Applying the same expansion (6) and collecting $O(\varepsilon)$ terms we obtain

$$-x_0' I_{0y} = I_{1yy} + S_1 I_0^2 + 2 S_0 I_0 I_1 - I_1, \tag{33}$$

where I_0 and S_0 are given by (13), (17b). We then multiply (33) by I_{0y} and integrate to obtain the solvability condition

$$x_0' \int_{-\infty}^{\infty} I_{0y}^2 dy = \frac{1}{3} \int_{-\infty}^{\infty} I_0^3 S_{1y} dy. \tag{34}$$

To determine S_{1y}, we match to the outer region. We expand

$$S(x; x_0) = S(x_0 + \varepsilon y; x_0) \sim S(x_0) + \varepsilon y S'(x_0^{\pm}) \text{ as } y \to \pm\infty, \tag{35}$$

where $S(x; x_0)$ in outer region is expressed in (13). Thus we obtain $S_{1y}(\pm\infty) = S'(x_0^{\pm})$. Taking the average we obtain

$$S_{1y} = -\frac{6\varepsilon}{S_0 D_S} \left(\frac{G_x(x_0^+; x_0) + G_x(x_0^-; x_0)}{2} \right) \tag{36}$$

where $G(x; x_0)$ is given in (11). Substituting (36) into (34) gives the equation that describes the motion of the interior spike:

$$x_0' = -\frac{6\varepsilon}{D_S S_0^2} \frac{\sinh\left(2\sqrt{\frac{\gamma}{D_R}} x_0\right)}{\sinh\left(2\sqrt{\frac{\gamma}{D_R}} L\right)}, \tag{37}$$

where S_0 is expressed in (17b). Write

$$S_0 = \varepsilon \hat{S}, \tag{38}$$

then we have

$$\frac{dx_0}{dt} = -\frac{6\varepsilon}{D_S \hat{S}^2} \frac{\sinh\left(2\sqrt{\frac{\gamma}{D_R}} x_0\right)}{\sinh\left(2\sqrt{\frac{\gamma}{D_R}} L\right)}. \tag{39}$$

Equation (39) has a zero equilibrium $x_0 = 0$. Its stability is determined by linearizing around $x_0 = 0$. The corresponding eigenvalue is computed by differentiating the right-hand side of (39) with respect to x_0 and evaluating it at zero: $\lambda = \partial_{x_0} \left(\frac{dx_0}{dt} \right)_{x_0=0}$. This yields

$$\lambda = -\frac{12\varepsilon}{D_S \hat{S}^2} \frac{\sqrt{\frac{\gamma}{D_R}}}{\sinh\left(2\sqrt{\frac{\gamma}{D_R}}L\right)} < 0. \tag{40}$$

Therefore the equilibrium centered at $x_0 = 0$ is stable with respect to spike motion.

4.1 Boundary effects and spike motion

From formula (40), it is clear that the eigenvalue is *stable*, provided that D_R is not too small. However numerical experiments show that the spike becomes unstable and moves to the boundary when D_R is sufficiently small (while other parameters are fixed). To understand this, note that for small D_R, (17b) simplifies to

$$S_0 \sim \frac{6\varepsilon\left(1+\frac{1}{\gamma}\right)}{N} \tag{41}$$

and $\hat{S} \sim \frac{6(1+\frac{1}{\gamma})}{N}$. Therefore (40) simplifies to

$$\lambda \sim -\frac{2}{3}\frac{\varepsilon N^2}{D_S\left(1+\frac{1}{\gamma}\right)^2}\sqrt{\frac{\gamma}{D_R}}\exp\left(-2L\sqrt{\frac{\gamma}{D_R}}\right), \quad D_R \ll 1 \tag{42}$$

so that the eigenvalue becomes exponentially small in D_R. On the other hand, there are also exponentially weak boundary effects due to the interaction of the pulse with the boundary that we disregarded in the computation leading to (34). These boundary terms appear when integrating by parts in (34). To compute them, we replace (34) by a more precise expression

$$-x_0' \int I_{0y}^2 dy = \left(I_{0y}I_{1y} - I_0 I_1\right)\Big|_{y=\frac{-L-x_0}{\varepsilon}}^{y=\frac{L-x_0}{\varepsilon}} + \int I_{0y} I_0^2 S_1 dy. \tag{43}$$

The computation of the boundary terms is relatively standard and we summarize it here. Note that

$$w(y) \sim 6e^{-y} \text{ as } y \to \infty \tag{44}$$

so that

$$I_0 \sim \frac{6}{S_0}\exp(-y). \tag{45}$$

For x near L, we change variables:

$$x = L + \varepsilon z$$

so that $y = \frac{L-x_0}{\varepsilon} + z$ and

$$I_0 \sim \frac{6}{S_0}\exp\left(-\frac{L-x_0}{\varepsilon}\right)\exp(-z). \tag{46}$$

Near $z = 0$, equation for I_1 satisfies $I_{1zz} - I_1 \sim 0$, so that $I_1 = A \exp z + B \exp(-z)$. Since $I'(L) = 0$, we must therefore have

$$I_1 \sim \frac{6\varepsilon}{S_0} \exp\left(-\frac{L - x_0}{\varepsilon}\right) \exp(z), \tag{47}$$

so that

$$(I_{0x} I_{1x} - I_0 I_1)|_{x=L} = -\frac{72\varepsilon}{S_0^2} \exp\left(-2\frac{L - x_0}{\varepsilon}\right). \tag{48}$$

Performing a similar computation at $x = -L$, and evaluating the remaining terms as before, we obtain

$$x_0' \sim -\frac{6\varepsilon}{D_S} \frac{\sinh\left(2\sqrt{\frac{\gamma}{D_R}} x_0\right)}{\sinh\left(2\sqrt{\frac{\gamma}{D_R}} L\right)} \frac{1}{\hat{S}^2} + 60\varepsilon \left\{\exp\left(2\frac{x_0 - L}{\varepsilon}\right) - \exp\left(2\frac{-L - x_0}{\varepsilon}\right)\right\} \tag{49}$$

so that

$$\lambda \sim -\frac{12\varepsilon}{D_S} \frac{\sqrt{\frac{\gamma}{D_R}}}{\sinh\left(2\sqrt{\frac{\gamma}{D_R}} L\right)} \frac{1}{\hat{S}^2} + 240 \exp\left(-\frac{2L}{\varepsilon}\right). \tag{50}$$

This expression clearly shows that the boundary term can play a destabilizing effect when the first term on the right hand side of (50) is exponentially small. This happens precisely when D_R is small. In this case, we estimate $\sinh\left(2\sqrt{\frac{\gamma}{D_R}} L\right) \sim \frac{1}{2} \exp\left(2\sqrt{\frac{\gamma}{D_R}} L\right)$ and (50) becomes

$$\lambda \sim -\frac{6\varepsilon}{D_S} \sqrt{\frac{\gamma}{D_R}} \frac{1}{\hat{S}^2} \exp\left(-2\sqrt{\frac{\gamma}{D_R}} L\right) + 240 \exp\left(-\frac{2L}{\varepsilon}\right).$$

Setting $\lambda = 0$, substituting $\hat{S} \sim \frac{6(1+\frac{1}{\gamma})}{N}$ and solving for D_S yields the critical value

$$D_S^* \sim \frac{\varepsilon N^2}{1440} \sqrt{\frac{\gamma}{D_R}} \frac{1}{(1 + \frac{1}{\gamma})^2} \exp\left(2L\left(\frac{1}{\varepsilon} - \sqrt{\frac{\gamma}{D_R}}\right)\right) \tag{51}$$

with a single spike centered at center being unstable when $D_S > D_S^*$, and stable otherwise. This phenomenon is illustrated in Fig. 2. Take $L = 1$, $\gamma = 1$, $N = 5$, $\varepsilon = 0.06$ and $D_R = 0.0059$. Then (51) yields $D_S^* = 5.00$. It follows that a single spike is unstable at the origin when $D_R < 0.0059$ and is stable otherwise. This is confirmed in Fig. 2.

The boundary effect discussed here is similar to destabilization discussed in Kolokolnikov and Ward (2004). However the difference here is that this effect is primarily driven by having a small D_R, and is very specific to having three components, and has no analogue as far as we know in the two-component RD systems.

In this section, in addition to D_R being small, we had to assume that $D_R \gg O(\varepsilon^2)$ in order to perform asymptotic calculations. However the same destabilization phenomenon is observed (numerically) even when $D_R = O\left(\varepsilon^2\right)$, although formula (51) is no longer valid there. It is an interesting open problem to show this analytically.

5 Instability thresholds of multi-spike equilibrium

In this section we study K-spike patterns, where $K \geq 1$. We analyze two types of instabilities, one is referred to as spike competition or coarsening instability, whereby some of the spikes are annihilated if the initial state contains too many spikes. The other is referred to as self replication, whereby a new spike may appear by the process of spike splitting. In this chapter we derive explicit thresholds for these instabilities.

5.1 Coarsening

When there are too many spikes, some of them get absorbed by others. This is known as coarsening or competition instability, and it occurs for example for sufficiently large value of D_S, while D_R is fixed independent of ε. To determine the instability threshold for spike competition, we apply the method in Kolokolnikov et al. (2012), Ward and Wei (2002) and compute the critical value at which an asymmetric spike pattern bifurcates from symmetric branch. To do this, consider a single interior spike on the domain $[-l, l]$. Duplicating the domain K times we obtain K spikes on the domain of size $2L = 2lK$. From (13) we have

$$S(x) = \frac{1}{D_S}\frac{6\varepsilon}{S_0}\left(G(0,0) - G(x;0)\right) + S_0, \tag{52}$$

Replacing L by l in (11) and evaluating (52) at $x = l$ we obtain

$$S(l) = S_0 + \frac{3\varepsilon}{D_S S_0}\sqrt{\frac{D_R}{\gamma}}\left(\frac{1}{\tanh\left(\sqrt{\frac{\gamma}{D_R}}l\right)} - \frac{1}{\sinh\left(\sqrt{\frac{\gamma}{D_R}}l\right)}\right), \tag{53}$$

where $S_0 = S_{0-}$ is given in (17b) with $x_0 = 0$. Plots of $S(l)$ when $D_S = 1$ and $D_S = 3$ are shown in Fig. 5. The bifurcation point corresponds to the minimum point of the curve $l \to S(l)$. Setting $S'(l) = 0$ then yields the critical stability threshold. Solving for D_S as a function of other parameters, and upon substituting $l = L/K$ we obtain the critical threshold

$$D_{SK}^{com} \sim \frac{N_0^2\left(\frac{L}{K}\right)^3}{3\varepsilon\left(1+\frac{1}{\gamma}\right)^2}\frac{\sinh s + 1}{\cosh s + 1}\frac{1}{s}, \quad \text{where } s = \sqrt{\frac{\gamma}{D_R}}\frac{L}{K}. \tag{54}$$

The K-spike solution is unstable and some of the spikes will disappear when $D_S > D_{SK}^{com}$. The plot of D_{SK}^{com} as a function of D_R is shown in Fig. 6. Note that D_{SK}^{com} has the following asymptotics as $D_R \to \infty$:

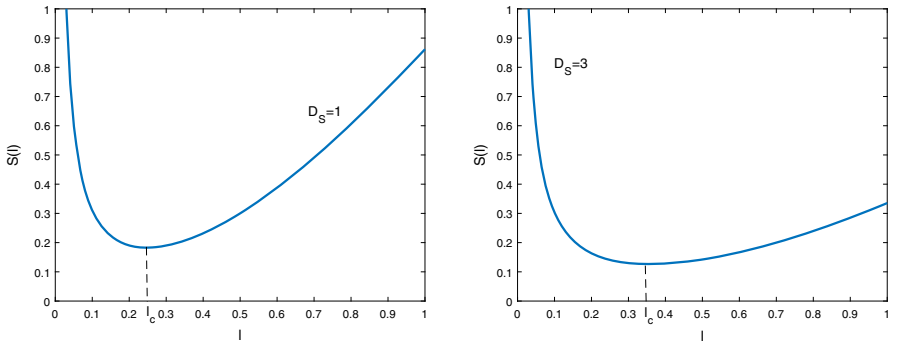

(a) $S(l)$ when $D_S = 1$ **(b)** $S(l)$ when $D_S = 3$

Fig. 5 Plots of function $S(l)$ versus l for $D_S = 1$ and $D_S = 3$. Other parameters are fixed and they are: $\varepsilon = 0.02$, $D_R = 2$, $\gamma = 1$, $N_0 = 4$

$$D_{SK}^{com} \sim \frac{N_0^2 \left(\frac{L}{K}\right)^3}{3\varepsilon \left(1 + \frac{1}{\gamma}\right)^2}, \text{ as } D_R \to \infty, \tag{55}$$

which is shown in Fig. 6. We now summarize the following result:

Result 5.1 *Consider a K-spike solution for the system (3) on an interval of length $2L$ with $K > 1$. Then in the limit of $\varepsilon \to 0$, this solution is stable provided that $D_S < D_{SK}^{com}$, where D_{SK}^{com} is given by (54). When $D_S > D_{SK}^{com}$, the K-spike solution becomes unstable due to competition (or coarsening) instability and some of the spikes disappear.*

5.2 Self-replication

Unlike coarsening instability, self-replication is related to disappearence of the single spike equilibrium solution. This instability occurs for example for when D_S is sufficiently small while D_R is fixed independent of ε. The mechanism has been studied in detail for Gray–Scott model (Doelman et al. 1997; Kolokolnikov et al. 2005c; Muratov and Osipov 2000, 2002; Reynolds et al. 1994, 1997), and it is similar here. We start by changing variables

$$S(x) = \frac{\varepsilon}{\sqrt{D_S}} \tilde{S}(x),\ I(x) = \frac{\sqrt{D_S}}{\varepsilon} \tilde{I}(x),\ x = \varepsilon y, \tag{56}$$

so that the system (3) transforms to

$$\begin{cases} \frac{\sqrt{D_S}}{\varepsilon} \tilde{S}_{yy} - \frac{\sqrt{D_S}}{\varepsilon} \tilde{S}\tilde{I}^2 + \gamma R = 0, \\ \tilde{I}_{yy} + \tilde{S}\tilde{I}^2 - \tilde{I} = 0, \\ \frac{D_R}{\varepsilon^2} R_{yy} + \frac{\sqrt{D_S}}{\varepsilon} \tilde{I} - \gamma R = 0. \end{cases} \tag{57}$$

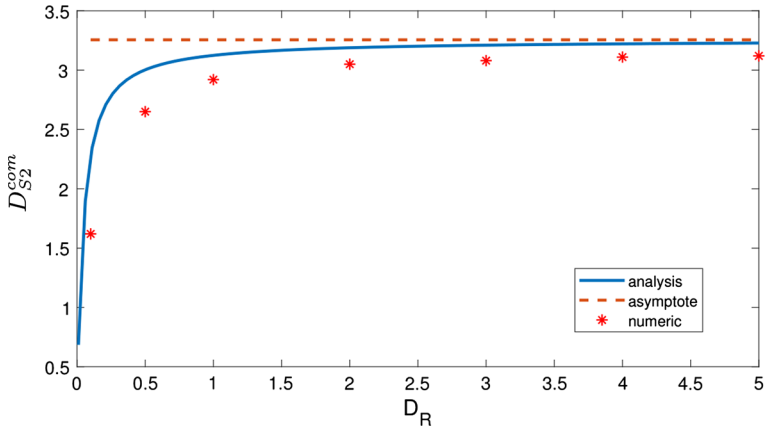

Fig. 6 Plot of stability threshold D_{S2}^{com} versus D_R for single spike solutions. Here $\varepsilon = 0.02$, $L = 1$, $N_0 = 2.5$, and $\gamma = 1$. The curve denotes analysis value D_{S2}^{com} obtained by (54), and the dashed line is the asymptote of the curve. The dots are obtained by numeric simulations, and they have a good agreement with analysis

Next, assume that D_S, D_R are $O(1)$. Then to leading order, in the inner region we obtain the following problem, referred to as the **core problem**,

$$\begin{cases} \tilde{S}_{yy} - \tilde{S}\tilde{I}^2 = 0, \\ \tilde{I}_{yy} + \tilde{S}\tilde{I}^2 - \tilde{I} = 0, \end{cases} \tag{58a}$$

this core problem is identical to the core problem for both the Grey–Scott model (Kolokolnikov et al. 2005c; Muratov and Osipov 2000, 2002; Reynolds et al. 1994), and the Schnakenberg model (Kolokolnikov and Wei 2018). Assuming that the spike is symmetric, we define

$$A := \tilde{S}_y(\infty) = \int_0^\infty \tilde{S}\tilde{I}^2 dy. \tag{58b}$$

By plotting the numerical bifurcation diagram of (58b), it was found in Kolokolnikov et al. (2005c) and Muratov and Osipov (2000) that the steady state disappears when $A > A_c \approx 1.35$, and this disappearence leads to self-replication. To determine A in terms of the other parameters of the problem, we perform an asymptotic matching to the outer region. We estimate $\int SI^2 = \int I$ and

$$D_R R_{xx} - \gamma R = -\left(\int I dx\right)\delta(x), \quad D_S S_{xx} + \gamma R = -\left(\int I dx\right)\delta(x).$$

The solution is then given by

$$R(x) = \frac{\left(\int I dx\right)}{D_R} G(x,0); \qquad S(x) = \frac{D_R}{D_S}\left(R(0) - R(x)\right), \tag{59a}$$

where $G(x)$ is as given in (11). We substitute (59) into the total mass equation (14) to obtain

$$N = 2N_0 l = 2A\sqrt{D_S}\left(1 + \frac{1}{\gamma} - \frac{D_R}{\gamma D_S}\right) + \frac{2Al}{\sqrt{D_S}} \frac{\sqrt{\frac{D_R}{\gamma}}}{\tanh\left(\frac{\gamma}{D_R} l\right)}, \tag{60}$$

so that self-replication occurs when

$$A = \frac{N_0 l \sqrt{D_S}}{D_S\left(1 + \frac{1}{\gamma}\right) + l \frac{\sqrt{\frac{D_R}{\gamma}}}{\tanh\left(\sqrt{\frac{\gamma}{D_R}} l\right)} - \frac{D_R}{\gamma}} > A_c \approx 1.35. \tag{61}$$

Equivalently, we rewrite (61) to obtain the following quadratic equation with respect to $\sqrt{D_S}$,

$$\left(1 + \frac{1}{\gamma}\right) D_S - \frac{N_0 l}{A_c}\sqrt{D_S} + \frac{\sqrt{\frac{D_R}{\gamma}} l}{\tanh\left(\sqrt{\frac{\gamma}{D_R}} l\right)} - \frac{D_R}{\gamma} = 0. \tag{62}$$

Self-replication of one-spike solution occurs when $D_S < D_S^{rep}$, where $\sqrt{D_S^{rep}}$ is the large root of (62). For K spikes on domain $[-L, L]$ with $L = Kl$, this leads to the following result:

Result 5.2 *Consider a K-spike solution of the system (3) on an interval of length $2L$ with $K \geq 1$. Then in the limit of $\varepsilon \to 0$, this solution is stable provided that $D_S > D_{SK}^{rep}$, where $D_S = D_{SK}^{rep}$ is the large root of (62), in which $l = \frac{L}{K}$ and $A_c \approx 1.35$ corresponds to the fold point of the problem (58).*

Figure 7 shows numerical validation of Result 5.2. The solid curve denotes the asymptotic curve as given in Result 5.2. Above the curve, a single spike is stable. As D_S is decreased and crosses the curve, self-replication takes place resulting in two spikes. The dots denote numeric simulations. Good agreement is observed between numerics and asymptotics.

For a fixed D_R and a given number of spikes K, we have derived both upper and lower thresholds on the D_S for which K spikes are stable. Note that multiple solutions (e.g. two or three spikes) can be stable at the same time. This is illustrated in Fig. 8.

6 Mesa-like steady states when $D_R = 0$

As shown in Sect. 5.1, multi-spike configurations lose stability when D_R is sufficiently small: even a single spike eventually becomes unstable (due to an exponentially small eigenvalue becoming positive) and moves towards the boundary when $D_R = O(\varepsilon^2)$. For even smaller values of D_R, we observe numerically that the spike "fattens" as shown in Fig. 9. In the limit of $D_R \to 0$, numerics indicate a phase separation of infected population. This can be thought of as a "quarantine effect": when mobility of recovered population and susceptible population is reduced, the infected population is confined to a certain region of the entire domain with a sharp interface inbetween.

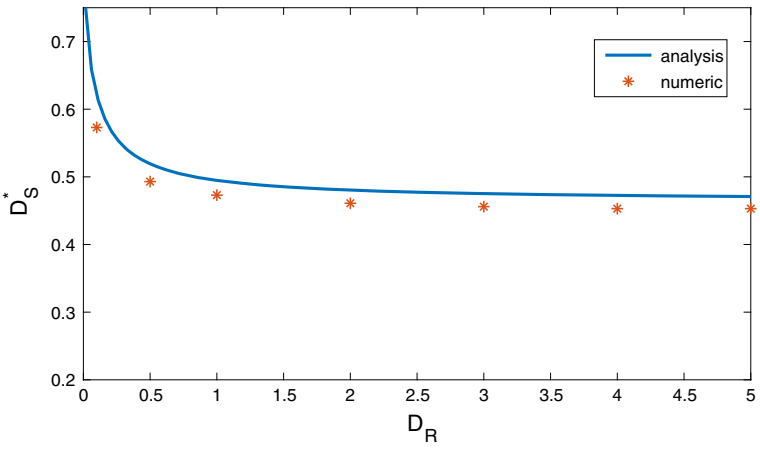

Fig. 7 Self-replication threshold (Result 5.2). Comparison between numerics and analysis. Solid curve is the analytical result given by (62). Dots denote numerical simulations. Self-replication is observed as D_S is decreased past the solid curve in the figure. Here $\varepsilon = 0.005$, $N = 5$, $L = 1$, and $\gamma = 1$.

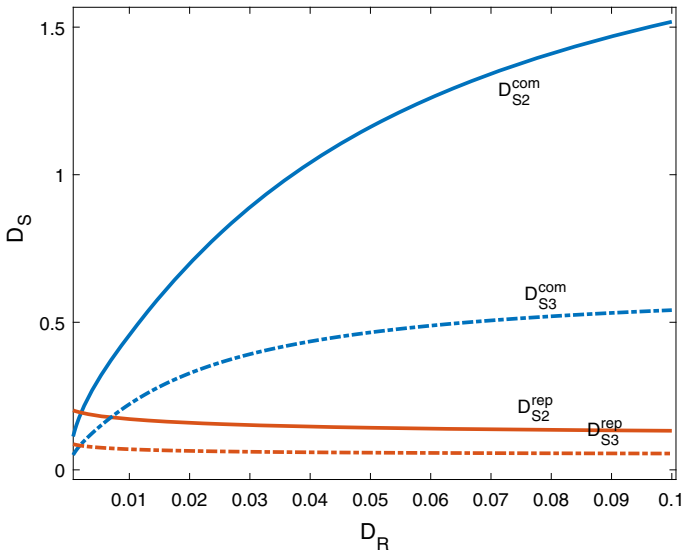

Fig. 8 Bifurcation diagram of K-spike patterns for $K = 2, 3$. The region between solid curves is the stable region for 2-spike patterns, and the region between dashed curves is the stable region for 3-spike patterns. Above the regions spike competition instability occurs, below the region, self replication instability occurs. Here $\varepsilon = 0.03$, $N_0 = 2.5$, $L = 1$, $\gamma = 1$

Here we perform the analysis for the limiting case $D_R = 0$ and D_S being small. At the steady state, we then have $I = \gamma R$ so that the model (3) reduces to

$$\begin{cases} 0 = D_S S_{xx} - SI^2 + I, \\ 0 = \varepsilon^2 I_{xx} + SI^2 - I. \end{cases} \tag{63}$$

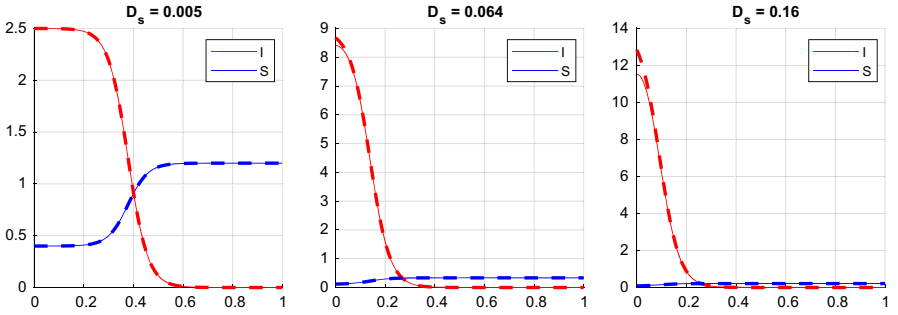

Fig. 9 Steady states of the system (3) with $L = 1$, $D_R = 0$, $\varepsilon = 0.04$, $\gamma = 1$, $N_0 = 2.79$ and with D_S as indicated. Solid curves correspond to the full numerical solution of (3). Dashed lines show the asymptotic approximation (67)

Adding the two equations we obtain that $D_S S + \varepsilon^2 I$ is constant. We then eliminate S from the second equation to obtain

$$D_S I_{xx} = \frac{D_S}{\varepsilon^2} I - C I^2 + I^3, \tag{64}$$

where

$$C = I + \frac{D_S}{\varepsilon^2} S \tag{65}$$

is a constant to be determined.

Equation (64) admits a heteroclinic solution connecting the steady state $I = 0$ to a positive steady state I_+ provided that the Maxwell-line condition holds: $\int_{I0}^{I_+} \left(\frac{D_S}{\varepsilon^2} I - C I^2 + I^3 \right) dI = 0$. This is equivalent to cubic having equidistant roots, that is,

$$\frac{D_S}{\varepsilon^2} I - C I^2 + I^3 = I \left(I - \frac{I_+}{2} \right) (I - I_+) \tag{66}$$

so that

$$I_+ = \sqrt{\frac{2 D_S}{\varepsilon^2}}, \quad C = \frac{3}{2} I_+. \tag{67a}$$

In this case there is an interface solution on the domain $[0, L]$ given by

$$\gamma R = I \sim I_+ \left(\frac{1}{2} \tanh \left(\frac{I_+}{2\sqrt{2}} \frac{(l - |x|)}{\sqrt{D_S}} \right) + \frac{1}{2} \right); \tag{67b}$$

$$S \sim \frac{\varepsilon^2}{D_S} I_+ \left(1 - \frac{1}{2} \tanh \left(\frac{I_+}{2\sqrt{2}} \frac{(l - |x|)}{\sqrt{D_S}} \right) \right). \tag{67c}$$

Here, l is the location of the interface. A back-to-back interface solution such as shown in Fig. 3 is obtained by extending this solution to $[-L, L]$ using even reflection. Finally, the interface location l is determined using the mass conservation condition, $N_0 L = \int_0^L (S + I + R) dx$. In the limit $\varepsilon \to 0$, this yields

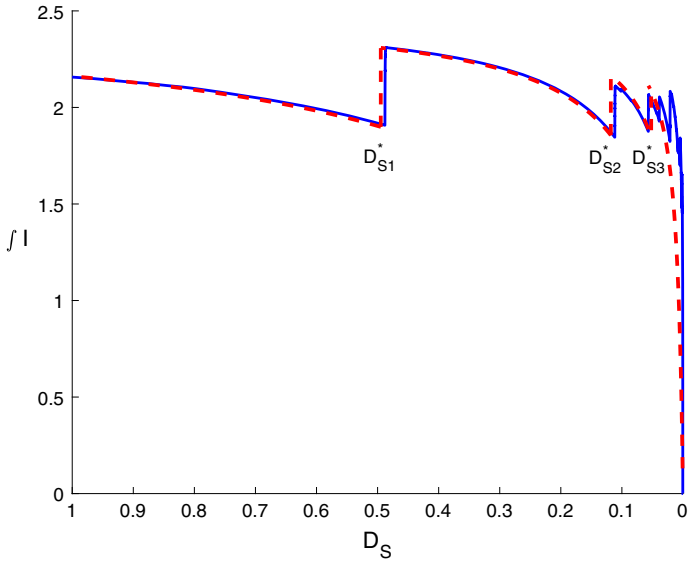

Fig. 10 Total mass of infected people versus D_S. Here $\varepsilon = 0.005$, $N = 5$, $D_R = 1$, $L = 1$, and $\gamma = 1$. The solid curve denotes numeric results, and dashed curves is the asymptotic result corresponding to self-replication thresholds of Result 5.2

$$LN_0 = I_+ \left\{ \left(1 + \frac{1}{\gamma}\right) l + \left(\frac{3}{2}L - \frac{1}{2}l\right)\left(\frac{\varepsilon^2}{D}\right) \right\}$$

so that solving for l we obtain

$$l = \frac{N_0 - I_+ \frac{3}{2}\left(\frac{\varepsilon^2}{D}\right)}{I_+\left(1 + \frac{1}{\gamma} - \left(\frac{\varepsilon^2}{D}\right)\right)} L. \tag{67d}$$

This result is valid as long as $O(\varepsilon) \ll l < L$. In this case, the interface has an exponentially weak effect on the boundary, and the agreement with the numerics is nearly perfect. Figure 9 illustrates this. Solution (67) is shown super-imposed on the numerical solution; the difference is imperceptible in the "eye-ball norm" as long as $l = O(1)$. The asymptotics break down when l becomes small (Fig. 9, right), and the interface transforms into a spike solution.

Note that the infected class subdivides the domain into outbreak portion ($x < l$) and disease-free portion ($x > l$). The susceptible population is three times smaller within the outbreak portion of the domain when compared with the disease-free portion.

For simplicity, we took $D_R = 0$ here. Numerical simulations indicate that similar interface solutions persist for sufficiently small D_R, although it changes l as well as the interface shape. We defer their study to future work.

7 Discussion

In this paper we studied the consequence of adding spatial diffusion to the relatively-standard SIRS model. Under certain reasonable assumptions, the resulting system (3) has a very rich solution space, exhibiting hot-spots as well as interface-type solutions, depending on whether D_R is large or small, respectively.

The analysis of drift instability when D_R is small in Sect. 4.1 was done for a single spike only. It would be interesting to see if this can be extended to multiple spikes. In the case of two spikes, this instability would presumably induce them to move towards each other until they merge. However in this case, there are *other* potential instabilities that are unique to multiple spikes (coarsening or competition instability), as discussed in Sect. 5.1. It is unclear which of these instabilities would dominate. Similarly, can self-replication occur for same parameter regimes as the drift instability of Sect. 4.1? These are interesting open questions for future work.

Occurrence of disease clusters has been widely documented in epidemiology literature, see e.g. Jeefoo (2012), Kruse et al. (2009), Otwombe (2014), Tanser et al. (2009) and Zulu et al. (2014). Our study underscores the importance of diffusion in formation of hot-spots and disease spread. One of the key assumptions leading to hot-spot formation was that the diffusion of infected class is relatively slow compared to the susceptible class. While it is difficult to measure (or even quantify) diffusion rates, one study (Tanser et al. 2009) did find a strong positive correlation between HIV hot-spot location and proximity to a large road. A multitutde of other causes have been proposed (see Otwombe 2014 and references therein). This includes the level of male circumcision; religiosity (less HIV prevalence in muslim communities in Africa); urbanization level with wider HIV prevalence in rural areas, among others; preponderence of drug use (Kruse et al. 2009).

The hot-spot regime $D_R \gg D_I$ is very similar to the previous analysis for the two-component reaction–diffusion systems, such as the Schnakenberg model (Kolokolnikov and Wei 2018; Ward and Wei 2002), and the behaviour is qualitatively similar to the SI model with diffusion introduced in Sun (2012) (which itself is a generalization of the Schnakenberg model). However, from the analysis point of view, the third component introduces a novel non-local eigenvalue problem (see Sect. 3). On the other hand, the regime $D_R \leq D_I$ requires completely new analysis. On one hand, the resolution of an exponentially small boundary layer in Sect. 4.1 is crucial for computing stability thresholds of a single interior spike in this regime. On the other, this regime also leads to mesa-type solutions of Sect. 6. The analysis there is similar to interface solutions derived in Hale et al. (1999) and Hale et al. (2000) for the Gray–Scott model. However it appears to be more robust: such interface solutions exist for a wide range of parameters here, rather than a very narrow range studied in Hale et al. (1999, 2000).

In Fig. 10 we plot the total mass of infected population versus D_S. As D_S is decreased, the mobility of susceptible population is reduced and initially leads to a decrease of overall disease load. However as D_S is decreased further, eventually a self-replication threshold is triggered. This results in an immediate increase of infection hot-spots and an overall increase in infected population. This underscores a highly nonlinear relationship between mobility and disease outbreaks.

Acknowledgements We would like to thank an anonymous referees for many useful suggestions which improved the exposition significantly. T.K. and D.I are funded by NSERC discovery grant. C.G. is funded in part by Nova Scotia Graduate Scholarship.

References

Arino J, Van den Driessche P (2003) A multi-city epidemic model. Math Popul Stud 10(3):175–193

Arino J, Jordan R, Van den Driessche P (2007) Quarantine in a multi-species epidemic model with spatial dynamics. Math Biosci 206(1):46–60

Buttenschoen A, Kolokolnikov T, Ward MJ, Wei J (2019) Cops-on-the-dots: the linear stability of crime hotspots for a 1-D reaction–diffusion model of urban crime. Europ J Appl Math. https://doi.org/10.1017/S0956792519000305

Doelman A, Kaper TJ, Zegeling PA (1997) Pattern formation in the one-dimensional gray–scott model. Nonlinearity 10(2):523

Doelman A, Gardner RA, Kaper TJ (2001) Large stable pulse solutions in reaction–diffusion equations. Indiana Univ Math J 50(1):443–507

Doran RJ, Laffan SW (2005) Simulating the spatial dynamics of foot and mouth disease outbreaks in feral pigs and livestock in Queensland, Australia, using a susceptible-infected-recovered cellular automata model. Prev Vet Med 70(1–2):133–152

Feng Z, Velasco-Hernández JX (1997) Competitive exclusion in a vector-host model for the dengue fever. J Math Biol 35(5):523–544

Fuks H, Lawniczak AT (2001) Individual-based lattice model for spatial spread of epidemics. Discrete Dyn Nat Soc 6(3):191–200

Hale JK, Peletier LA, Troy WC (1999) Stability and instability in the gray–scott model: the case of equal diffusivities. Appl Math Lett 12(4):59–65

Hale JK, Peletier LA, Troy WC (2000) Exact homoclinic and heteroclinic solutions of the gray–scott model for autocatalysis. SIAM J Appl Math 61(1):102–130

Hethcote HW (2000) The mathematics of infectious diseases. SIAM Rev 42(4):599–653

Iron D, Ward MJ (2002) The dynamics of multispike solutions to the one-dimensional gierer–meinhardt model. SIAM J Appl Math 62(6):1924–1951

Iron D, Ward MJ, Wei J (2001) The stability of spike solutions to the one-dimensional gierer–meinhardt model. Phys D Nonlinear Phenom 150(1):25–62

Jeefoo P (2012) Spatial patterns analysis and hotspots of hiv/aids in Phayao province, Thailand. Arch Des Sci 65(9):37–50

Kang K, Kolokolnikov T, Ward MJ (2007) The stability and dynamics of a spike in the one-dimensional keller-segel model. IMA J. Appl. Math 72(2):140–162

Kermack WO, McKendrick AG (1927) A contribution to the mathematical theory of epidemics. Proc R Soc Lond Ser A Contain Papers Math Phys Character 115(772):700–721

Kolokolnikov T, Ward MJ (2004) Bifurcation of spike equilibria in the near-shadow gierer–meinhardt model. DSDS B 4:1033–1064

Kolokolnikov T, Wei J (2018) Pattern formation in a reaction–diffusion system with space-dependent feed rate. SIAM Rev 60(3):626–645

Kolokolnikov T, Ward MJ, Wei J (2005a) The existence and stability of spike equilibria in the one-dimensional gray–scott model on a finite domain. Appl Math Lett 18(8):951–956

Kolokolnikov T, Ward MJ, Wei J (2005b) The existence and stability of spike equilibria in the one-dimensional gray–scott model: the low feed-rate regime. Stud Appl Math 115(1):21–71

Kolokolnikov T, Ward MJ, Wei J (2005c) The existence and stability of spike equilibria in the one-dimensional gray–scott model: the pulse-splitting regime. Phys D Nonlinear Phenom 202(3–4):258–293

Kolokolnikov T, Ward M, Wei J (2012) The stability of steady-state hot-spot patterns for a reaction–diffusion model of urban crime. arXiv preprint arXiv:1201.3090

Kruse GR, Barbour R, Heimer R, Shaboltas AV, Toussova OV, Hoffman IF, Kozlov AP (2009) Drug choice, spatial distribution, HIV risk, and HIV prevalence among injection drug users in St. Petersburg, Russia. Harm Reduct J 6(1):22

Kuperman M, Abramson G (2001) Small world effect in an epidemiological model. Phys Rev Lett 86(13):2909
Lamb Jr GL (1980) Elements of soliton theory. Wiley, New York
Lloyd AL, Jansen VAA (2004) Spatiotemporal dynamics of epidemics: synchrony in metapopulation models. Math Biosci 188(1–2):1–16
Maini PK, Woolley TE, Baker RE, Gaffney EA, Lee SS (2012) Turing's model for biological pattern formation and the robustness problem. Interface Focus 2:487–496
Muratov CB, Osipov VV (2000) Static spike autosolitons in the gray–scott model. J Phys A Math General 33(48):8893
Muratov CB, Osipov VV (2002) Stability of the static spike autosolitons in the gray–scott model. SIAM J Appl Math 62(5):1463–1487
Murray JD (2001) Mathematical biology. II Spatial models and biomedical applications, Interdisciplinary applied mathematics, vol 18. Springer, New York
Otwombe LA (2014) Spatial distribution and analysis of factors associated wiyh HIV infection among young people in Eastern Africa: applied to the MEASURE demographic and health survey data collected between 2007 and 2011. PhD thesis
Painter KJ, Hillen T (2011) Spatio-temporal chaos in a chemotaxis model. Phys D Nonlinear Phenom 240(4):363–375
Reynolds WN, Pearson JE, Ponce-Dawson S (1994) Dynamics of self-replicating patterns in reaction diffusion systems. Phys Rev Lett 72(17):2797
Reynolds WN, Ponce-Dawson S, Pearson JE (1997) Self-replicating spots in reaction–diffusion systems. Phys Rev E 56(1):185
Sherratt JA, Lord GJ (2007) Nonlinear dynamics and pattern bifurcations in a model for vegetation stripes in semi-arid environments. Theor Popul Biol 71(1):1–11
Sun G-Q (2012) Pattern formation of an epidemic model with diffusion. Nonlinear Dyn 69(3):1097–1104
Tanser F, Bärnighausen T, Cooke GS, Newell M-L (2009) Localized spatial clustering of hiv infections in a widely disseminated rural south african epidemic. Int J Epidemiol 38(4):1008–1016
van den Driessche P, Watmough J (2000) A simple SIS epidemic model with a backward bifurcation. J Math Biol 40(6):525–540
Ward MJ, Wei J (2002) The existence and stability of asymmetric spike patterns for the schnakenberg model. Stud Appl Math 109(3):229–264
Wei J (1999) On single interior spike solutions of the gierer–meinhardt system: uniqueness and spectrum estimates. Eur J Appl Math 10(4):353–378
Wei J, Winter M (2013) Mathematical aspects of pattern formation in biological systems. Springer, Berlin
Yuan H, Chen G (2008) Network virus-epidemic model with the point-to-group information propagation. Appl Math Comput 206(1):357–367
Zulu LC, Kalipeni E, Johannes E (2014) Analyzing spatial clustering and the spatiotemporal nature and trends of hiv/aids prevalence using gis: the case of malawi, 1994–2010. BMC Infect Dis 14(1):285